Optical absorption of hyperbolic metamaterial with stochastic surfaces

Jingjing Liu,[1] Gururaj V. Naik,[1,2] Satoshi Ishii,[1,3] Clayton DeVault,[4] Alexandra Boltasseva,[1,5] Vladimir M. Shalaev,[1] and Evgenii Narimanov[1,*]

[1]*School of Electrical and Computer Engineering and Birck Nanotechnology Center, Purdue University, West Lafayette, Indiana 47907, USA*
[2]*Department of Materials Science and Engineering, Stanford University, Stanford, California 94305, USA*
[3]*National Institute of Information and Communications Technology, Nishi-ku, Kobe 651-2492, Japan*
[4]*Department of Physics, Purdue University, West Lafayette, Indiana 47907, USA*
[5]*DTU Fotonik, Department of Photonics Engineering, Technical University of Denmark, Lyngby, DK-2800, Denmark*
[*]*evgenii@jpurdue.edu*

Abstract: We investigate the absorption properties of planar hyperbolic metamaterials (HMMs) consisting of metal-dielectric multilayers, which support propagating plane waves with anomalously large wavevectors and high photonic-density-of-states over a broad bandwidth. An interface formed by depositing indium-tin-oxide nanoparticles on an HMM surface scatters light into the high-k propagating modes of the metamaterial and reduces reflection. We compare the reflection and absorption from an HMM with the nanoparticle cover layer versus those of a metal film with the same thickness also covered with the nanoparticles. It is predicted that the super absorption properties of HMM show up when exceedingly large amounts of high-k modes are excited by strong plasmonic resonances. In the case that the coupling interface is formed by non-resonance scatterers, there is almost the same enhancement in the absorption of stochastically perturbed HMM compared to that of metal.

OCIS codes: (250.5403) Plasmonics; (160.3918) Metamaterials; (300.1030) Absorption.

References and links

1. J. B. Pendry, "Negative refraction makes a perfect lens," Phys. Rev. Lett. **85**(18), 3966–3969 (2000).
2. N. Fang, H. Lee, C. Sun, and X. Zhang, "Sub-diffraction-limited optical imaging with a silver superlens," Science **308**(5721), 534–537 (2005).
3. Z. Jacob, L. V. Alekseyev, and E. Narimanov, "Optical Hyperlens: Far-field imaging beyond the diffraction limit," Opt. Express **14**(18), 8247–8256 (2006).
4. A. Salandrino and N. Engheta, "Far-field subdiffraction optical microscopy using metamaterial crystals: Theory and simulations," Phys. Rev. B **74**(7), 075103 (2006).
5. D. Schurig, J. J. Mock, B. J. Justice, S. A. Cummer, J. B. Pendry, A. F. Starr, and D. R. Smith, "Metamaterial electromagnetic cloak at microwave frequencies," Science **314**(5801), 977–980 (2006).
6. R. Atkinson, W. R. Hendren, G. A. Wurtz, W. Dickson, A. V. Zayats, P. Evans, and R. J. Pollard, "Anisotropic optical properties of arrays of gold nanorods embedded in alumina," Phys. Rev. B **73**(23), 235402 (2006).
7. J. Yao, Z. W. Liu, Y. M. Liu, Y. Wang, C. Sun, G. Bartal, A. M. Stacy, and X. Zhang, "Optical negative refraction in bulk metamaterials of nanowires," Science **321**(5891), 930 (2008).
8. M. A. Noginov, Y. A. Barnakov, G. Zhu, T. Tumkur, H. Li, and E. E. Narimanov, "Bulk photonic metamaterial with hyperbolic dispersion," Appl. Phys. Lett. **94**(15), 151105 (2009).
9. A. J. Hoffman, L. Alekseyev, S. S. Howard, K. J. Franz, D. Wasserman, V. A. Podolskiy, E. E. Narimanov, D. L. Sivco, and C. Gmachl, "Negative refraction in semiconductor metamaterials," Nat. Mater. **6**(12), 946–950 (2007).
10. Z. Jacob, J. Y. Kim, G. V. Naik, A. Boltasseva, E. E. Narimanov, and V. M. Shalaev, "Engineering photonic density of states using metamaterials," Appl. Phys. B **100**(1), 215–218 (2010).
11. G. V. Naik, J. J. Liu, A. V. Kildishev, V. M. Shalaev, and A. Boltasseva, "Demonstration of Al:ZnO as a plasmonic component for near-infrared metamaterials," Proc. Natl. Acad. Sci. U.S.A. **109**(23), 8834–8838 (2012).

12. G. V. Naik, B. Saha, J. Liu, S. M. Saber, E. Stach, J. Irudayaraj, T. D. Sands, V. M. Shalaev, and B. A., "A Titanium Nitride based Metamaterial for Applications in the Visible," in *Conference on Lasers and Electro-Optics/Quantum Electronics and Laser Science and Photonic Applications Systems Technologies*, Technical Digest (CD) (Optical Society of America, 2013), paper QTu3A.7.
13. T. Tumkur, G. Zhu, P. Black, Y. A. Barnakov, C. E. Bonner, and M. A. Noginov, "Control of spontaneous emission in a volume of functionalized hyperbolic metamaterial," Appl. Phys. Lett. **99**(15), 151115 (2011).
14. H. N. S. Krishnamoorthy, Z. Jacob, E. Narimanov, I. Kretzschmar, and V. M. Menon, "Topological Transitions in Metamaterials," Science **336**(6078), 205–209 (2012).
15. M. Y. Shalaginov, S. Ishii, J. Liu, J. Liu, J. Irudayaraj, A. Lagutchev, A. V. Kildishev, and V. M. Shalaev, "Broadband enhancement of spontaneous emission from nitrogen-vacancy centers in nanodiamonds by hyperbolic metamaterials," Appl. Phys. Lett. **102**(17), 173114 (2013).
16. D. Lu, J. J. Kan, E. E. Fullerton, and Z. W. Liu, "Enhancing spontaneous emission rates of molecules using nanopatterned multilayer hyperbolic metamaterials," Nat. Nanotechnol. **9**(1), 48–53 (2014).
17. C. Simovski, S. Maslovski, I. Nefedov, and S. Tretyakov, "Optimization of radiative heat transfer in hyperbolic metamaterials for thermophotovoltaic applications," Opt. Express **21**(12), 14988–15013 (2013).
18. Z. W. Liu, H. Lee, Y. Xiong, C. Sun, and X. Zhang, "Far-field optical hyperlens magnifying sub-diffraction-limited objects," Science **315**(5819), 1686 (2007).
19. E. Narimanov, M. Noginov, H. Li, and A. Barnakov, "Darker than Black: Radiation-absorbing Metamaterial," in *Conference on Lasers and Electro-Optics/Quantum Electronics and Laser Science and Photonic Applications Systems Technologies*, Technical Digest (CD) (Optical Society of America, 2010), paper QPDA6.
20. T. U. Tumkur, J. K. Kitur, B. Chu, L. Gu, V. A. Podolskiy, E. E. Narimanov, and M. A. Noginov, "Control of reflectance and transmittance in scattering and curvilinear hyperbolic metamaterials," Appl. Phys. Lett. **101**(9), 091105 (2012).
21. E. E. Narimanov, H. Li, Y. A. Barnakov, T. U. Tumkur, and M. A. Noginov, "Reduced reflection from roughened hyperbolic metamaterial," Opt. Express **21**(12), 14956–14961 (2013).
22. E. M. Purcell, "Spontaneous Emission Probabilities at Radio Frequencies," Phys. Rev. **69**, 681 (1946).
23. Z. F. Yu, A. Raman, and S. H. Fan, "Fundamental limit of nanophotonic light trapping in solar cells," Proc. Natl. Acad. Sci. U.S.A. **107**(41), 17491–17496 (2010).
24. W. L. Barnes, "Fluorescence near interfaces: the role of photonic mode density," J. Mod. Opt. **45**(4), 661–699 (1998).
25. S. Rytov, "Electromagnetic properties of a finely stratified medium," Sov. Phys. JETP **2**, 466–475 (1956).
26. S. Franzen, "Surface plasmon polaritons and screened plasma absorption in indium tin oxide compared to silver and gold," J. Phys. Chem. C **112**(15), 6027–6032 (2008).
27. C. Rhodes, S. Franzen, J. P. Maria, M. Losego, D. N. Leonard, B. Laughlin, G. Duscher, and S. Weibel, "Surface plasmon resonance in conducting metal oxides," J. Appl. Phys. **100**(5), 054905 (2006).
28. C. Guclu, S. Campione, and F. Capolino, "Hyperbolic metamaterial as super absorber for scattered fields generated at its surface," Phys. Rev. B **86**(20), 205130 (2012).

1. Introduction

Metamaterials are artificially engineered structures with subwavelength features whose optical properties transcend those found in nature. Due to their unique electromagnetic response, metamaterials have generated many new and exciting applications such as perfect lenses [1, 2], hyperlenses [3, 4], and invisibility cloaking [5].

One particular class of metamaterials which has become the research focus is hyperbolic metamaterials (HMMs). The two most common structures used to realize an HMM are metallic nanowires embedded in a dielectric matrix [6–8] and periodic planar metal-dielectric layers [9–12]. These uniaxial media with the elements of the permittivity tensor $\varepsilon = diag(\varepsilon_\perp, \varepsilon_\parallel, \varepsilon_\parallel)$ being parallel ($\varepsilon_\parallel$) and perpendicular ($\varepsilon_\perp$) to the sample surface are highly anisotropic and exhibit hyperbolic dispersion as $\varepsilon_\perp$ and $\varepsilon_\parallel$ are simultaneously of opposite sign. This is evident by considering the dispersion relation $\dfrac{k_\perp^2}{\varepsilon_\parallel} + \dfrac{k_\parallel^2}{\varepsilon_\perp} = \dfrac{\omega^2}{c^2}$ where the subscripts "$\parallel$" and "$\perp$" respectively indicate the direction parallel and perpendicular to the sample surface. For dielectric terms having opposite signs (i.e. $\varepsilon_\perp > 0$ and $\varepsilon_\parallel < 0$ or $\varepsilon_\parallel > 0$ and $\varepsilon_\perp < 0$), the dispersion relation becomes a hyperbola as opposed to an ellipse found in conventional materials. Due to the mutilayered subwavelength composition, the hyperbolic dispersion of HMMs is not a resonance-dependent phenomenon.

One of the interesting consequences of hyperbolic dispersion is the anomalous large photonic density of states which has already shown new physical phenomena such as radiative decay enhancement [10, 12–16], heat transport [17], and imaging [3, 18]. One particular implementation of HMMs is their use to enhance absorption [19–21]. Fundamentally, absorption into an HMM may be understood in terms of Fermi's Golden Rule [22] which claims the scattering rate into a particular mode is proportional to that mode's density of state. Hence, for a scatterer placed in the vicinity of an HMM, light will preferentially scatter into the HMM. Both periodically patterned nanostructures and stochastic surfaces are capable of providing the missing momentum required to couple light from free space [23]. Periodically patterned structures generally operate in a narrow bandwidth and are easily perturbed by defects, while stochastic surfaces do not have such bandwidth limitations due to their random surface distribution.

There have been several attempts to use stochastically perturbed surface as the coupler between free space and metamaterial devices. The stochastic surface opens routes for light to span the available high-k states, suppress the back reflection, and increase the light coupling efficiency. Reduced reflection and scattering was proposed using an HMM with a roughened surface [19]. In the experimental paper by Tumkur et al [20], the reflection was moderately reduced when stochastic surfaces were introduced to the HMM formed by silver/MgF$_2$ multilayers.

However, it is well known that a roughed metal surface would also show suppressed reflection. Light scattered by textured interfaces decays in the form of surface plasmon polaritons and lossy surface waves [24]. The decay routes introduced by the scattering events implement the energy transfer from the stochastic surface to the subsequent metal film. The facts make the stochastically textured metal film a competitive well absorbing medium. Thus, there is a need for detailed studies of optical losses in an HMM as compared to a metal film.

In this paper, a detailed study of controlling the reflection and absorption by stochastic surfaces formed on HMMs and metal films is presented and possible mechanisms are discussed. The nanoparticles are randomly dispersed on top of an HMM surface to form a stochastic interface layer. The multiple scattering events from nanoparticles are utilized to couple free space light into the HMM and the metal. In this work, we use epitaxially grown titanium nitride (TiN), aluminum scandium nitride ((Al,Sc)N) superlattice to form HMMs, and the stochastic surface is introduced by indium-tin-oxide (ITO) nanoparticles.

2. Experiment

Metal/dielectric superlattice is epitaxially grown to form 10 ultrathin and smooth alternating layers, each with a thickness of 10 nm on a [001] MgO substrate [12]. TiN is a plasmonic material that grows epitaxially on MgO [001] and Al$_{0.72}$Sc$_{0.28}$N grows lattice matched on TiN. Thus, the HMM is composed of TiN as the metallic material and (Al,Sc)N as the dielectric material; (Al,Sc)N dielectric layer is the top-most layer. The optical properties of the superlattice were characterized using a spectroscopic ellipsometer (J.A. Woollam Co) at three angles of incidence 30°, 45° and 60° [11]. Because of the superlattice with the layer thickness much smaller than the wavelength, the effective permittivity tensor is uniaxial and may be

approximated as $\varepsilon_{\|} = p\varepsilon_{\text{TiN}} + (1-p)\varepsilon_{(\text{Al,Sc})\text{N}}$, $\varepsilon_{\perp} = \dfrac{\varepsilon_{\text{TiN}}\,\varepsilon_{(\text{Al,Sc})\text{N}}}{(1-p)\varepsilon_{\text{TiN}} + p\varepsilon_{(\text{Al,Sc})\text{N}}}$, where ε_{TiN} and

$\varepsilon_{(\text{Al,Sc})\text{N}}$ are the permittivities of the TiN and (Al,Sc)N layers respectively, and p is the metal filling ratio [25]. The effective permittivity tensor of the superlattice, as retrieved from the ellipsometry measurements, is shown in Fig. 1(a), 1(b). Our superlattice metamaterial exhibits opposite signs of real permittivity in different directions for wavelengths longer than 520 nm. The iso-frequency surface in the k-space undergoes a transition from elliptical to hyperbolic shape when the sign of $\text{Re}(\varepsilon_{\|}\varepsilon_{\perp})$ changes from positive to negative, and thus qualifies our

material as a HMM for wavelengths longer than 520 nm. $\varepsilon_{\parallel}^{'} > 0$ and $\varepsilon_{\perp}^{'} < 0$ for wavelengths between 520 nm and 620 nm qualifies the supperlattice as a transverse positive HMM. And $\varepsilon_{\parallel}^{'} < 0$ and $\varepsilon_{\perp}^{'} > 0$ for wavelengths longer than 620 nm qualifies it as a transverse negative HMM. The permittivity of the TiN film is also retrieved from the separate ellipsometry measurement and shown in Fig. 1(c).
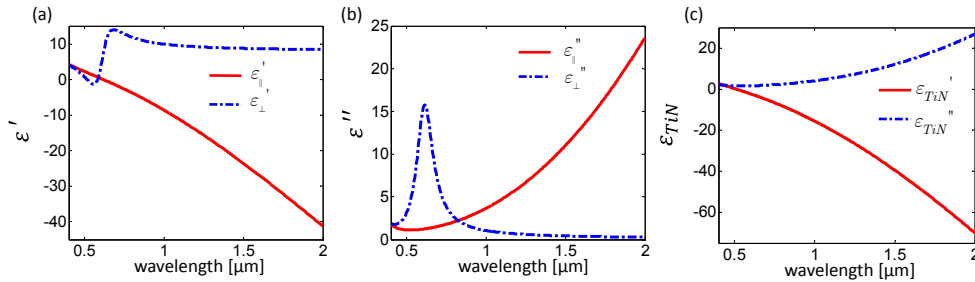

Fig. 1. The real part (a) and imaginary part (b) of permittivity of the TiN/(Al,Sc)N HMM retrieved by spectroscopic ellipsometry. (c) The real and imaginary part of permittivity of the TiN film.
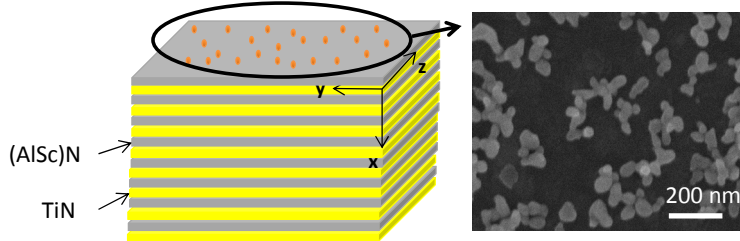

Fig. 2. Schematic of multi-layered metal/dielectric HMM and SEM image of the HMM spin-coated with15 μL of diluted -ITO suspension.

A schematic of the multi-layer metal/dielectric and an SEM image of the stochastic surface are shown in Fig. 2. The stochastic surface is created by spin-coating ITO nanoparticles on top of the HMM surface. ITO particles used in this research consisted of 90 wt % indium oxide (In_2O_3) and 10 wt % tin oxide (SnO_2) with mean particle size of 50 nm. They were dispersed in isopropyl alcohol to form 30 wt % suspension of ITO nanoparticles (purchased from Sigma Aldrich). The suspension was then sixty times diluted by isopropyl alcohol, and 15 μL of this liquid was spin coated on the TiN/(Al,Sc)N HMM superlattice at 2500 rpm in the duration of 30 seconds. The same process for producing stochastic surfaces was repeated on the same thickness TiN film. The diffused reflectance $R(\omega)$ from each sample was measured at an 8° incident angle in a wavelength range from 400 nm to 2 μm using a Lambda-950 (Perkin Elmer Co.) spectrometer with an integrating sphere. Both the specular reflection and the backward scattering were collected by the integrating sphere. The diffused transmittance $T(\omega)$ was measured at normal incidence. Again both the transmission and the forward scattering were collected. Finally, the absorption was calculated as $1 - R(\omega) - T(\omega)$.

Figure 3(a) shows that the reflectance of the TiN/ (Al,Sc)N HMM is less than that of TiN over all wavelengths. As 15 μL of the diluted ITO solutions is applied, diffused reflectance of both the HMM and TiN (denoted in the figure as HMM-ITO-1 and TiN-ITO-1 respectively) decreased with a corresponding increase in absorption. The procedure of spin-coating the ITO nanoparticle suspension was repeated six more times to study if there would be any drastic

modification of absorption. As six fold increase of ITO particle densities on the surface, diffused reflectance (denoted in the figure as HMM-ITO-2 and TiN-ITO-2) further dropped down for wavelengths longer than 650 nm for HMM, but increased for shorter wavelengths. This variation is understood as the backward scattering from the ITO particles compensate the absorption loss of HMM and the ITO particles. TiN also shows similar behavior, except that the transition happens at 545 nm wavelength. In addition, ITO particles are metallic-like in the wavelengths longer than 1.4 μm [26, 27]. So a valley appears in the reflectance for the sample coated with the six fold increase of ITO particles which are equivalent to a rough ITO film.
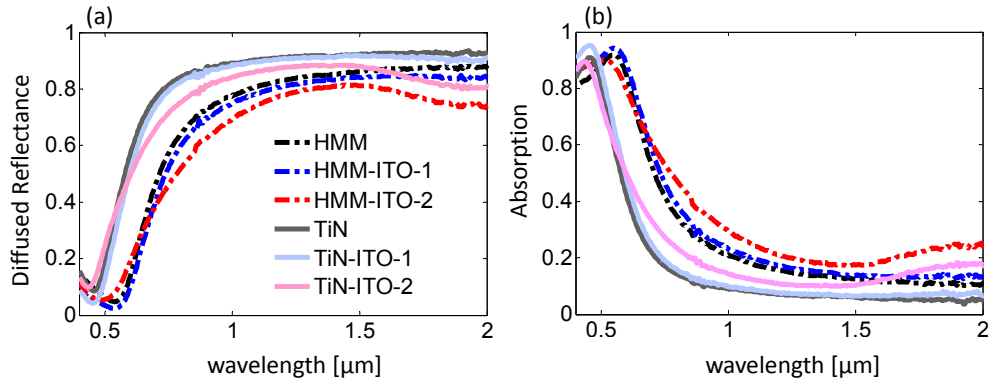

Fig. 3. Diffused reflectance (a) and absorption (b) of TiN/(Al,Sc)N HMM, TiN film and ITO coated HMM and ITO coated TiN film.

3. Discussion

It should be noted that ITO particles introduce almost the same incremental absorption in HMM and TiN for both cases. To investigate the absorption process, we simulate the scattering by an ITO particle on top of the HMM and TiN films. As shown in the SEM image of the HMM-ITO-1 (Fig. 2), only one layer of particles covers the top surface. In general, the ITO-particles are touching each other, however do not aggregate heavily. To simplify our simulations, we independently consider each particle as a sphere on top of HMM and neglect the multi-sphere interactions, because it is known that the effects of particle interactions and particle shapes are strong only at resonance. In non-resonant condition, neglecting inter-particle interaction and shape variations produces little discrepancy and well follows the experimental data. The discrepancy due to this approximation especially for wavelength longer than 1.5 μm will be discussed in later section. In the case of HMM/TiN-ITO-2, most particles are heavily aggregating and render more simulation difficulties. Furthermore, there are no additional interesting distinguishments between the absorption behaviors of HMM and TiN away from the transition regions. Therefore, we limit the simulation settings for the first case (HMM/TiN-ITO-1). In our simulation set-up (Fig. 4(a)), a single spherical ITO particle is placed directly on top of the HMM and TiN film surface. TiN/(Al,Sc)N HMM is treated as a binary layered medium. The dielectric function of the ITO particle is described using a Drude model with the permittivity plot shown in Fig. 4(b). A mesh size of 1 nm in the vicinity of the ITO particle is used. The calculation domain is bounded by perfectly matched layers. A plane wave is normally incident on the sample polarized in the z direction.

The pronounced properties of the HMM rely on propagating waves with anomalously large wave vectors arising from the scattering events on the particle-HMM interface. Similarly, scattering generates surface plasmon polaritons (SPPs) on the air/TiN interface, accompanied by the appearance of high-k waves. To evaluate the distributions of the scattered field in the k space, we perform 2D Fourier transform of the E_z component of the scattered

field on the particle-film interface and 20 nm below the interface (Fig. 4). Two representative wavelengths 0.8 µm and 2 µm are chosen for calculations. It may be noticed that there is an asymmetric distribution between directions of k_y and k_z, since the incident field is polarized in the z direction and the four-fold symmetry is not maintained. Furthermore, there is a clear distinction in the k-space scattering distributions between HMM and TiN. For HMM, field magnitudes of low-k waves are suppressed, and high-k waves above a certain edge are propagating. The field distribution on the TiN film is spread over all the k space, and also covering a large k space area. To understand the k-space scattering maps explicitly, we plot dispersion diagrams obtained by Bloch theory in Fig. 5(a). We observe that the real part of $k_\perp (k_x)$ versus $k_\parallel (k_{y,z})$ resembles an opening hyperbola shape. The high anisotropy greatly suppresses the propagation in a region (i.e. bandgap) spanning from $k_\parallel \sim 0$ to $3k_0$. Above the region, long range propagation exists inside HMM. This is compared with TiN (Fig. 5(b)) where iso-frequency surface is towards a closed ellipse, hence there are equal probabilities for waves to scatter across a continuously large k space area.

In addition, at 2 µm wavelength we obtain a much more broad field distribution in the k space (Fig. 4(e)) due to the intense localized surface plasmon resonance (LSPR) supported by air/ITO/HMM environment. And after propagating one period of superlattice (Fig. 4(g)), the high-k waves are substantially decaying, but still predominant. We do not observe LSPR from the HMM coated with 15 µL diluted ITO suspension, since multiple scatterings events will broaden the resonance width and eventually smear it out.

To conclude, the distribution of the scattering fields in k space follows the same trend found in the iso-frequency surface. As the iso-frequency surface of HMM becomes transverse negative hyperbolic dispersion, a wider range of wave vectors appear, which is also concluded in references [10, 14, 15]. The photonic states opened by the scattering events on the stochastic surfaces will be coupled into the HMM. Since loss in the metal introduces a decay constant, these modes do eventually get absorbed. On the metal film, the stochastic surface formed by the ITO particles also couples light to high-k waves as illustrated. The majority of high-k waves are lost by internal absorption which involves the energy transfer from high-k waves to a variety of energy decay processes in metal [24].

To calculate the absorption power of the HMM and TiN due to the ITO particle scattering, we integrate the dissipation power density for the scattered field over the occupied volume. The absorption is calculated as dividing the absorption power by the incident power on the geometrical cross section of the particle. Figure 6(a) shows the absorption by the TiN/(Al,Sc)N HMM and TiN film for the scattering fields. The transition wavelength (λ = 620 nm) marked by the thin black arrow, distinguishes the transverse positive hyperbolic dispersion from the transverse negative. As indicated by the permittivity plot (Fig. 1(c)) of the TiN film, the air/TiN interface supports strong SPPs resonance close to the wavelength of 550 nm. Thus, TiN absorbs more than HMM does. Above the transition wavelength, HMM absorbs more than TiN, and reaches a peak at 1.9 µm. The power absorbed by the ITO particle is calculated by integrating the dissipation power density for the full field over the particle volume as shown in Fig. 6(b). The absorption of the ITO particle is dependent on the substrate configurations. Larger absorption is found when the particle is sitting on top of the HMM. Since the ITO particle becomes metallic around 1.4 µm as shown in Fig. 4(b), LSPR starts to play a role beyond this point. Due to the dielectric component of the permittivity tensor of HMM, LSPR of the ITO particle is expected to be stronger, and results in much higher absorption. It might be noted that the ITO particle plays the dominant role of overall absorption above the transition wavelength (λ = 620 nm).
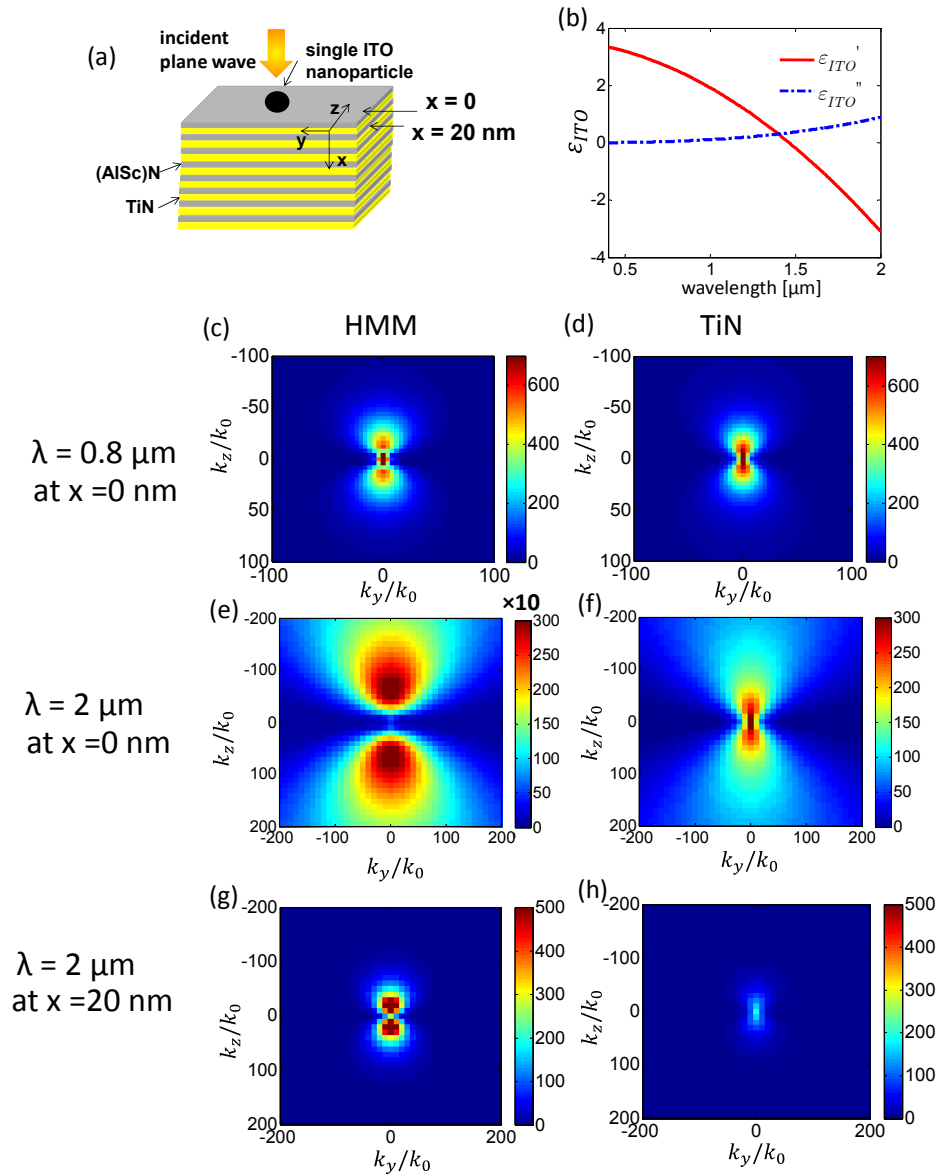
Fig. 4. (a) The simulation setup. A single spherical ITO particle is placed on top of the film surface. (b) The real and imaginary part of permittivity of the ITO particle. A plane wave is normally incident on the sample polarized in the z direction. (c-h) display maps of the E_z component of the scattering field in the k space (k_y, k_z) at the wavelength of 0.8 μm and 2 μm. (c-f) are drawn on the particle-film interface and (g, h) are drawn 20 nm below the interface.
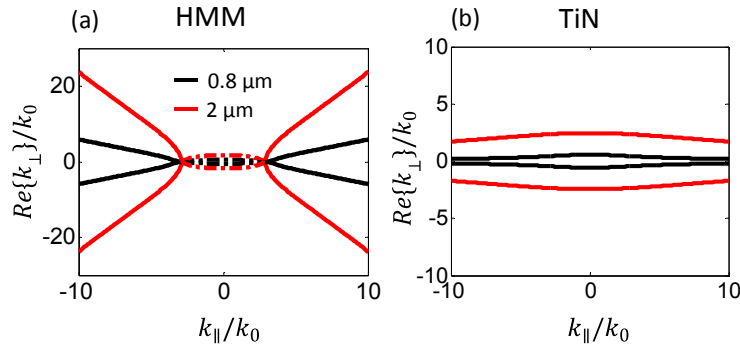
Fig. 5. Iso-frequency surfaces of HMM (a) and TiN (b). $\text{Re}(k_\perp)$ is plotted against $k_\parallel$ at the wavelength of 0.8 μm and 2 μm obtained by Bloch theory. The dashed ellipse in (a) is the propagating suppression region (i.e. bandgap) in k space for HMM.

We also evaluate the scattering efficiency of the ITO sphere to make a comparison with Reference [28] which uses silver/silica HMM for the purpose of absorbing scattered fields generated by silver nanoparticle. In our case, the scattering efficiency is 2.9×10^{-3} for an ITO nanosphere on top of TiN/(AlSc)N HMM at the wavelength of 0.8 μm. This is consistent with the result of Reference [28] where single silver nanosphere is placed on top of silver/silica HMM.

The absorption of the samples coated with 15 μL ITO suspension can be estimated by adding the absorption by the films, the absorption by the films due to the particle scattering (data shown in Fig. 6(a)) and absorption of the ITO particle (data shown in Fig. 6(b)). Here we neglect the interference between the background fields and the scattered fields, and also the interactions between particles. The assumption is only valid when the particle-substrate interactions and particle-particle interactions are much smaller than the background fields. This assumption will not be true if strong LSPR takes place in the system. As shown in Fig. 6(c) the simulation fits reasonably well with the measurements before LSPR takes an action, but deviates considerably for wavelengths longer than 1.5 μm. Experimentally, this can be understood as multiple particle scatterings very much broaden the single particle resonance. The particle layer effectively behaves as an impedance buffered medium, and slightly reduces the back reflection. In addition, the simulation predicts that the exotic properties of HMM will show up when strong plasmonic resonance occurs such as LSPR.
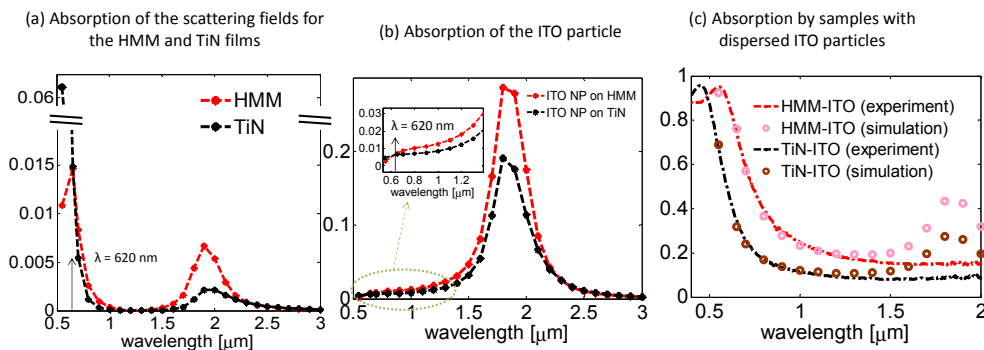

Fig. 6. (a) Calculated absorption of scattered fields in TiN/(Al,Sc)N HMM and TiN film. The absorption is calculated by dividing the absorbed power by the incident power on the geometrical cross section of the particle. (b) Calculated absorption of the ITO nanoparticle on top of the HMM and TiN films. The inset shows the magnified figure for wavelengths from 0.55 μm to 1.3 μm. (c) Measured and calculated absorption spectra of the HMM and TiN films with dispersed ITO particles.

4. Conclusion

In conclusion, the experiment conveys a message that there is almost the same amount of absorption of an HMM compared to that of a metal film, when both of them are covered by a stochastic coupling surface formed by non-resonant scatterers. The propagating modes and high-k modes in the metal consume comparatively the same amount of scattering power with HMM. The simulation predicts the super absorption properties of HMM when exceedingly large amounts of high-k modes are excited. It could be achieved by strong plasmonic resonance such as LSPR.

Acknowledgment